Effects of band structure and quantum interference on the differential conductance of infinite metallic single-wall carbon nanotubes

2007 J. Phys.: Condens. Matter 19 096207

(http://iopscience.iop.org/0953-8984/19/9/096207)

IOP PUBLISHING JOURNAL OF PHYSICS: CONDENSED MATTER

J. Phys.: Condens. Matter **19** (2007) 096207 (19pp) doi:10.1088/0953-8984/19/9/096207

Effects of band structure and quantum interference on the differential conductance of infinite metallic single-wall carbon nanotubes

M Bagheri[1,4] **and A Namiranian**[2,3]

[1] Physics Department, Shahid Beheshti University, Evin, Tehran 19839, Iran
[2] Computational Physical Science Laboratory, Department of Nano-Science, Institute for Studies in Theoretical Physics and Mathematics (IPM), P.Box 19395-5531, Tehran, Iran
[3] Physics Department, Iran University of Science and Technology, Narmak, Tehran 16345, Iran

E-mail: mh-bagheri@cc.sbu.ac.ir

Received 12 October 2006, in final form 15 January 2007
Published 14 February 2007
Online at stacks.iop.org/JPhysCM/19/096207

Abstract

Using a π-orbital tight-binding (TB) model within a perturbative formalism, the effects of substitutional impurities on the conductance of infinite metallic single-wall carbon nanotubes (MSWCNTs) are studied. The perturbative scheme is based on the energy dissipation of electrons travelling through the nanotube. A general expression for the differential conductance (DC) is presented, and scattering processes are investigated. It is demonstrated how the DC depends sensitively on the nature of the electronic band structure and velocity of carriers moving in the nanotube. We have shown that the quantum interference (QI) of electronic waves scattered by impurities plays a meaningful role. In particular, for the case of a couple of impurities the DC exhibits periodic oscillations comprising both positive and negative values. The negative differential conductance (NDC) stemming from the QI and rotational symmetry selection rule is very sensitive to the relative distance and symmetry of two impurities. This signature is absent for the case of a single impurity. In fact, the NDC can be attributed to the *zero-temperature/elastic weak-localization* correction to the conductance. As a result, *the faster/higher* and *slower/shorter* oscillations can then effectively be achieved by *metallic zigzag* and *armchair* nanotubes, respectively.

(Some figures in this article are in colour only in the electronic version)

[4] Author to whom any correspondence should be addressed.

1. Introduction

Since their discovery in the last decade by Iijima [1], carbon nanotubes have received much attentions owing in a large part to their peculiar quasi-one-dimensional structures and unique electronic properties. Carbon nanotubes can be considered as seamless cylinders made of a two-dimensional graphene sheet rolled up along the chiral vector. This vector is indexed by two integers (n, m) and connects crystallographically equivalent sites. Depending sensitively on the diameter and helicity, which are uniquely determined by the chiral vector, electronic band structure calculations predict metallic or semiconducting behaviours. If $n - m = 3q$, with $q = 0, \pm 1, \pm 2, \ldots$ the tubes are metallic; otherwise they are semiconducting [2–5].

Quantum transport in carbon nanotube systems has intensively attracted numerous considerations due to suitable potential applications for nanodevices [6–11]. The most commonly used computational scheme to treat the problem of quantum transport in such systems is based on the Landauer approach that relates the electronic conductance to the transmission coefficient [12]. The transmission function is usually obtained within the Green's function scattering formalism coupled with a simple TB model [13, 14]. In SWCNTs, the TB π-orbital formalism is a qualitatively useful and simple model to obtain the conductance, because its electronic structure information can be straightforwardly calculated [15]. The number of subbands which contribute to the conductance is related to the threshold voltage determining whether a channel is opened or closed. These calculations predict the conductance quantization for a perfect metallic nanotube in the case of ideal contacts. Because of the two conducting channels crossing at the Fermi energy, the maximum amount of the conductance of ballistic transport reaches $2G_0$, where $G_0 = 2e^2/h$ is the conductance quantum [2, 16]. However, contrary to the perfect nanotube case, several theoretical results [17–25] and experimental evidences [26–29] have shown that in the presence of structural disorders such as Stone–Wales [30], substitutional impurities, vacancies, and adsorbates the quantized conductance of the nanotube does not follow the aforementioned results. In particular, Choi *et al* [19] have demonstrated that *ab initio* results are sometimes quite different from a single-band π-orbital TB calculations. Usually, in manufacturing and manipulation nanotubes into devices a few imperfections naturally arise, and investigation of their influences on the transport characteristics has evolved to be a field of very active research. For all imperfections, the moving carriers scatter, and the electrical conductance of the device will usually decrease. From a practical point of view, studying the quantum conductance of defective SWCNTs provides a significant opportunity to realize their useful device applications. It is shown that the scattering in an ideal metallic SWCNT is extremely reduced, while in a doped semiconductor SWCNT an electron can be backscattered [23, 24].

In this work, we have developed a toy model presented in [31] to a more realistic one so as to investigate the electron scattering processes in MSWCNTs. More precisely, this paper addresses the following: how the band structure of an MSWCNT affects the QI induced by electronic waves scattered by not-charged substitutional impurities. We assume that the Fermi energy level remains unchanged at the charge neutrality point (CNP), where the bonding and antibonding bands cross. It then preserves the electron–hole symmetry. However, the conductance is very sensitive to the type of nanotube band structure and location of the Fermi energy. In reality, the conductance can be changed by shifting the Fermi energy from the CNP due to doping or a gate voltage. In order to investigate transport properties of MSWCNTs, the DC is derived by using a fairly different approach: a perturbative scheme based on the rate of energy dissipation of moving electrons through the nanotube [31–33]. A general expression for the DC versus an external source–drain potential has been extracted. We have found that in the case of a pair of impurities the DC as a function of the source–drain voltage exhibits

a periodically oscillatory behaviour resulting from the QI effects. The most important feature is that the DC shows negative values in both bias directions, and it depends sensitively on the spatial configurations of impurities over the tubular surface. In fact, it manifests that QI effects, which are responsible for localization and resonant phenomena in 1D systems, play a prominent role in the context of carbon nanotubes. This is important due to a very specific band structure of nanotubes consisting of many one-dimensional subbands with a spacing determined by the tube radius. These properties may be exploited for the quantum interference devices based on metallic nanotubes. In recent years, different mechanisms of the NDC have been reported in various structures of nanotubes [34–37]. Practically, the NDC has many applications including memory, high-speed atomic switching, and amplifications. This signature is absent in the case of a single impurity.

The paper is organized as follows. In section 2, we briefly develop a TB model for describing the band structure of the nanotube. We have derived two expressions for the band structure and Bloch's wavefunction in the framework of the zone-folding approximation. In our case, the current is produced by π-orbital electrons travelling in the crystalline field under a small source–drain voltage. The general features of the transport around the Fermi level can be well explained by the π-orbital approximation. Curvature effects are not included, and a δ-function potential is assumed to include the interaction of electrons with impurities. Eventually, a multi-band equation for the DC for arbitrary number of subbands and arbitrary number of impurities located at arbitrary positions is obtained. In section 3, we discuss backscattering processes in metallic nanotubes. In section 4, analytical calculations are supported by numerical results together with a brief discussion on the findings. Finally, a conclusion is given in section 5.

2. Model

We investigate electronic transport in a model system consisting of an MSWCNT in the presence of impurities and an axial external bias. A typical configuration of the geometry used can be found in [2]. To describe the electronic structure of the system we use a single-orbital nearest-neighbours tight-binding (NNTB) approach. It includes the localized π-orbital of carbon atoms on the nanotube. The Hamiltonian of the entire system is

$$\hat{\mathcal{H}} = \hat{\mathcal{H}}_{\text{tube}} + \hat{\mathcal{H}}_{\text{sd}} + \hat{\mathcal{H}}_{\text{imp}}. \tag{1}$$

The first term describing the kinetic energy of electrons for a perfect nanotube can be written as follows [38]:

$$\hat{\mathcal{H}}_{\text{tube}} = \sum_{\alpha=\pm} \sum_{q=1}^{N_t/2} \sum_{k\in}^{\text{FBZ}} \mathcal{E}_q^{\alpha}(k) \hat{C}_q^{\dagger\alpha}(k) \hat{C}_q^{\alpha}(k), \tag{2}$$

in which $\mathcal{E}_q^{\pm}(k)$ denotes the band structure of a typical nanotube (n, m). It is given by

$$\frac{\mathcal{E}_q^{\pm}(k)}{\gamma_0} = \pm \left\{ 1 + 4\cos\left[\frac{\sqrt{3}}{2} a_{cc}\left(\frac{q}{r_t}\sin\omega + k\cos\omega\right)\right]\cos\left[\frac{3}{2} a_{cc}\left(\frac{q}{r_t}\cos\omega - k\sin\omega\right)\right] + 4\cos^2\left[\frac{\sqrt{3}}{2} a_{cc}\left(\frac{q}{r_t}\sin\omega + k\cos\omega\right)\right]\right\}^{\frac{1}{2}}, \tag{3}$$

where the operators $\hat{C}_q^{\dagger\pm}(k)$ and $\hat{C}_q^{\pm}(k)$ create/destroy electrons in the orbital with energy $\mathcal{E}_q^{\pm}(k)$. The $-$ and $+$ signs correspond to the valence (π) and conduction (π^*) band, respectively. Good quantum numbers (ignoring the spin degree of freedom everywhere) of

electron states are (q, k), with $q = 1, \ldots, N_t/2$ and $k \in (-\pi/T, \pi/T)$. The quantity N_t counts the number of carbon atoms in the nanotube unit cell, and $\mathcal{N} \equiv N_t/2$ turns out to be the number of graphene unit cells in a given nanotube unit cell. r_t and $a_{cc} \simeq 1.44$ Å stand for the nanotube radius and C–C bond length, respectively. Also, $\omega = \pi/6 - \theta$, in which θ is the chiral angle of the nanotube. For armchair nanotubes $\theta = \pi/6$, but for the zigzag ones $\theta = 0$. The quantity $\gamma_0 \simeq 3.0$ eV is the nearest-neighbour overlap integral energy. For simplicity, on-site energies are set to zero. Furthermore, all metallic linear bands in a nanotube cross the undoped Fermi level ($\mathcal{E}_{\mathcal{F}} = 0$) either degenerated at $k_{\mathrm{F}} = 0$ (metallic zigzag) or separated at $k_{\mathrm{F}} = \pm 2\pi/3T$ (armchair) in the first Brillouin zone (FBZ). The corresponding electronic states of an isolated nanotube with discrete subband index q and continuous longitudinal wavevector k in terms of the atomic functions can be found to be

$$|q, k; \zeta\rangle = \frac{1}{\sqrt{2\mathcal{M}\mathcal{N}}} \sum_{l} \sum_{j} \Omega(q, k; \vec{C}_h, \vec{T}, \vec{R}_j) \times \mathrm{e}^{\mathrm{i}lTk} \left[\Gamma\left(\frac{q}{r_t}, k\right) |\vec{T}_l, \vec{R}_j, \vec{d}_1\rangle + \zeta |\vec{T}_l, \vec{R}_j, \vec{d}_2\rangle \right], \tag{4}$$

where

$$\Omega(q, k; \vec{C}_h, \vec{T}, \vec{R}_j) = \exp\left(\mathrm{i}\left[\frac{q}{r_t}\left(\vec{R}_j \cdot \frac{\vec{C}_h}{C_h}\right) + k\left(\vec{R}_j \cdot \frac{\vec{T}}{T}\right)\right]\right), \tag{5}$$

and

$$\Gamma\left(\frac{q}{r_t}, k\right) = \frac{\Upsilon(\frac{q}{r_t}, k)}{|\Upsilon(\frac{q}{r_t}, k)|}, \tag{6}$$

in which $\Upsilon(\vec{k}) = 1 + \mathrm{e}^{-\mathrm{i}\vec{k}\cdot\vec{a}_1} + \mathrm{e}^{-\mathrm{i}\vec{k}\cdot\vec{a}_2}$. Note that $\vec{k} = (k_x, k_y)$, where $k_x = (q/r_t)\cos\omega - k\sin\omega$ and $k_y = (q/r_t)\sin\omega + k\cos\omega$. In equation (4), the basis $|\vec{T}_l, \vec{R}_j, \vec{d}_\mu\rangle$ represents the atomic orbital centred at a site located at the atomic position $\vec{d}_\mu$ of the hexagonal unit cell $\vec{R}_j$ in the nanotube unit cell l. The first sum goes over the nanotube unit cells and the second one counts the nodes within a given nanotube unit cell. The quantity $\mathcal{M}$ represents the total number of nanotube unit cells as well. All geometrical information relevant to the nanotube is now accessible in this picture. Furthermore, $\zeta = \pm 1$ is a pseudospin discerning between the states of the valence and conduction bands. The pseudospinor vector is formed by a two-component complex amplitude of the wavefunction defined for two atoms (A and B) in the graphite unit cell. It is not the electrons spin, but it represents the sublattice. Taking into account the pseudospinor vector instead of the plane wave state might be the reason for the long mean free path in metallic nanotubes [23, 39, 40].

To include the influence of the external source–drain voltage on electrons, the second term in equation (1) can be written as follows [31, 41, 42]:

$$\hat{\mathcal{H}}_{\mathrm{sd}} = \frac{eV_{\mathrm{sd}}}{2} \sum_{\alpha=\pm} \sum_{q=1}^{N_t/2} \sum_{k\in}^{\mathrm{FBZ}} \mathrm{sign}[v_q^\alpha(k)] \hat{C}_q^{\dagger\alpha}(k) \hat{C}_q^\alpha(k), \tag{7}$$

where $v_q^\pm(k) = (1/\hbar)\partial\mathcal{E}_q^\pm(k)/\partial k$ is the electron velocity. In equation (7), we have assumed that the nanotube is infinite to assure that the electric field inside the nanotube far from its ends is negligible and the energy of ballistic electrons depends only on the sign of velocity along the nanotube axis. It is also supposed that $eV_{\mathrm{sd}} \ll \mathcal{E}_{\mathrm{F}}$ and that the nanotube is smoothly connected to the macroscopic reservoirs.

The last term in equation (1) is the Hamiltonian of the interaction of electrons with impurities. It is represented by [37, 41]

$$\hat{\mathcal{H}}_{\rm imp} = \sum_{\alpha,\beta=\pm} \sum_{q,q'=1}^{N_t/2} \sum_{k,k'\in}^{\rm FBZ} \sum_{\xi=1}^{r} J^{qq'}_{\xi,\alpha\beta}(k,k')\hat{C}^{\dagger\alpha}_{q}(k)\hat{C}^{\beta}_{q'}(k'), \tag{8}$$

where $J^{qq'}_{\xi,\alpha\beta}(k,k')$ (hereafter the **J**-function) is a matrix of dimension 2×2 for the impurity potential located at a position, namely, $\vec{x}_\xi$. It is defined as follows:

$$J^{qq'}_{\xi,\alpha\beta}(k,k') = \langle \alpha; q, k|\hat{V}_{\rm imp}(\vec{x}-\vec{x}_\xi)|q', k'; \beta\rangle, \tag{9}$$

where $\hat{V}_{\rm imp}(\vec{x}-\vec{x}_\xi)$ is the operator of the single-impurity potential, with $\alpha = \pm$ and $\beta = \pm$. For simplicity, as a model of a scatterer we consider a point-like impurity, i.e. $\hat{V}_{\rm imp}(\vec{x}-\vec{x}_\xi) = g\delta_{\vec{x},\vec{x}_\xi}$, in which g is the impurity strength, and δ is the Kronecker delta function. The matrix elements of the scattering potential between the Bloch's states describe the scattering amplitudes. We emphasize that our formalism is quite general and can be used with more complicated impurity potentials such as extended, charged impurities, and ionized dopants. After a simple but cumbersome algebra the diagonal and off-diagonal elements of the scattering potential are, respectively,

$$\begin{aligned} J^{qq'}_{\xi,\alpha\alpha}(k,k') = {} & \frac{g}{2\mathcal{M}\mathcal{N}} \sum_{l}\sum_{R_j} {\rm e}^{{\rm i}lT(k'-k)}\Omega^*(q,k;\vec{C}_h,\vec{T},\vec{R}_j)\Omega(q',k';\vec{C}_h,\vec{T},\vec{R}_j) \\ & \times \left(\Gamma^*\left(\frac{q}{r_t},k\right)\Gamma\left(\frac{q'}{r_t},k'\right)\delta_{\vec{x}_\xi,\vec{T}_l+\vec{R}_j+\vec{d}_1} + \delta_{\vec{x}_\xi,\vec{T}_l+\vec{R}_j+\vec{d}_2}\right), \end{aligned} \tag{10}$$

$$\begin{aligned} J^{qq'}_{\xi,\alpha\beta}(k,k') = {} & \frac{g}{2\mathcal{M}\mathcal{N}} \sum_{l}\sum_{R_j} {\rm e}^{{\rm i}lT(k'-k)}\Omega^*(q,k;\vec{C}_h,\vec{T},\vec{R}_j)\Omega(q',k';\vec{C}_h,\vec{T},\vec{R}_j) \\ & \times \left(\Gamma^*\left(\frac{q}{r_t},k\right)\Gamma\left(\frac{q'}{r_t},k'\right)\delta_{\vec{x}_\xi,\vec{T}_l+\vec{R}_j+\vec{d}_1} - \delta_{\vec{x}_\xi,\vec{T}_l+\vec{R}_j+\vec{d}_2}\right), \end{aligned} \tag{11}$$

where $J^{qq'}_{\xi,\alpha\alpha}(k,k') = [J^{q'q}_{\xi,\alpha\alpha}(k',k)]^*$. Also, $J^{qq'}_{\xi,\alpha\beta}(k,k') = J^{qq'}_{\xi,\beta\alpha}(k,k')$ and $J^{qq'}_{\xi,\alpha\alpha}(k,k') = J^{qq'}_{\xi,\beta\beta}(k,k')$. For plane wave states the matrix element is just the Fourier transform, so the **J**-function is the factor carrying the information from the Bloch states. Let us assume $\vec{x}_\xi = \vec{T}_{l''} + \vec{R}_{j''} + \vec{d}_\nu$, in which $\nu = 1, 2$. In the case when the impurity is located at site A (B), the second (first) term in equations (10) and (11) is equal to zero.

In order to investigate the influence of impurities on the nonlinear quantum conductance, we have now employed the method based on the perturbation theory and second quantization representation of the Hamiltonian developed by Kulik *et al* [32, 33]. The change in the electric current ΔI is related to the rate of the energy dissipation by the following relation:

$$\Delta I V_{\rm sd} = \frac{{\rm d}E}{{\rm d}t} = \frac{{\rm d}\langle\hat{\mathcal{H}}_{\rm sd}\rangle}{{\rm d}t}; \tag{12}$$

by means of the Heisenberg equation of motion one can obtain the differential of $\langle\hat{\mathcal{H}}_{\rm sd}\rangle$. Thus, the change in ΔI owing to the interaction of electrons with impurities is given by

$$\Delta I V_{\rm sd} = \frac{1}{{\rm i}\hbar}\left\langle[\hat{\mathcal{H}}_{\rm sd}(t), \hat{\mathcal{H}}_{\rm imp}(t)]\right\rangle, \tag{13}$$

where

$$\left\langle\hat{\mathcal{O}}\right\rangle = {\rm Tr}\left(\hat{\rho}(t)\hat{\mathcal{O}}\right). \tag{14}$$

All operators are in the Dirac representation. The density operator $\hat{\rho}(t)$ satisfies the following equation of motion:

$$\mathrm{i}\hbar\frac{\partial\hat{\rho}(t)}{\partial t} = [\hat{\mathcal{H}}_{\mathrm{imp}}(t), \hat{\rho}(t)]. \tag{15}$$

Equation (15) can be solved iteratively for $\hat{\rho}(t)$ for the arbitrary $\hat{\mathcal{H}}_{\mathrm{sd}}$ but using perturbation in $\hat{\mathcal{H}}_{\mathrm{imp}}(t)$. It reads as follows:

$$\hat{\rho}(t) = \hat{\rho}_0 + \frac{1}{\mathrm{i}\hbar}\int_{-\infty}^{\infty}\mathrm{d}t_1\Theta(t-t_1)[\hat{\mathcal{H}}_{\mathrm{imp}}(t_1), \hat{\rho}_0]. \tag{16}$$

Substituting the expression given by equation (16) for the density operator up to the second order in the impurity potential leads to

$$\Delta I = \frac{-1}{\hbar^2 V_{\mathrm{sd}}}\int_{-\infty}^{\infty}\mathrm{d}t_1\Theta(t-t_1)\mathrm{Tr}\Big\{\hat{\rho}_0\Big[[\hat{\mathcal{H}}_{\mathrm{sd}}(t), \hat{\mathcal{H}}_{\mathrm{imp}}(t)], \hat{\mathcal{H}}_{\mathrm{imp}}(t_1)\Big]\Big\}. \tag{17}$$

The above equation essentially includes correlation and coherence effects which cannot be described by the first order in the impurity potential. We define the decrease in the total conductance, i.e. $\Delta G \equiv -G_{\mathrm{imp}}$, as follows:

$$G_{\mathrm{imp}} = -\frac{\mathrm{d}(\Delta I)}{\mathrm{d}V_{\mathrm{sd}}}. \tag{18}$$

Upon substituting equations (7) and (8) into (17), and by exploiting the standard single-particle Green's function approach, we find (see appendix A)

$$\begin{aligned}\Delta I^{\alpha\alpha}(V_{\mathrm{sd}}) = \frac{\pi e}{\hbar}\sum_{q=1}^{N_t/2}\sum_{q'=1}^{N_t/2}\sum_{k\in}^{\mathrm{FBZ}}\sum_{k'\in}^{\mathrm{FBZ}}\sum_{\xi=1}^{r}\sum_{\eta=1}^{r} J^{qq'}_{\xi,\alpha\alpha}(k,k')J^{q'q}_{\eta,\alpha\alpha}(k',k)\\ \times\,\delta\left[\mathcal{E}^{\alpha}_{q}(k)-\mathcal{E}^{\alpha}_{q'}(k')\right]\left[\mathrm{sign}[v^{\alpha}_{q}(k)]-\mathrm{sign}[v^{\alpha}_{q'}(k')]\right]\\ \times\,\left\{n_{\mathrm{F}}\left[\mathcal{E}^{\alpha}_{q}(k)+\frac{eV_{\mathrm{sd}}}{2}\mathrm{sign}[v^{\alpha}_{q}(k)]\right]-n_{\mathrm{F}}\left[\mathcal{E}^{\alpha}_{q'}(k')+\frac{eV_{\mathrm{sd}}}{2}\mathrm{sign}[v^{\alpha}_{q'}(k')]\right]\right\};\end{aligned} \tag{19}$$

as expected, the total current becomes $\Delta I^{\alpha\alpha}_{\mathrm{total}} = \Delta I^{++} + \Delta I^{--}$. Owing to the orthonormality condition, $\Delta I^{\alpha\beta} = 0$. Equation (19) shows that the current is determined by four factors: 1—the availability of states, given by the difference of occupation numbers; 2—the velocity of carriers within the states; 3—the **J**-function determining the QI effects; 4—the type of the band structure.

Moreover, the electrochemical potential of the reservoir at the left (right) end is $\mu_{\mathrm{L}}(\mu_{\mathrm{R}})$. To set up the transport of electrons through the nanotube, the electrochemical potentials μ_{L} and μ_{R} are shifted relatively so as to create a slight imbalance. We define eV_{sd} as the energy window between two electrochemical potentials. Each reservoir injects electrons with an energy whose accessibility is checked by the Fermi distribution function $n_{\mathrm{F}}[\mathcal{E}^{\alpha}_{q}(k)-\mu] = [\mathrm{e}^{[\mathcal{E}^{\alpha}_{q}(k)-\mu]/k_{\mathrm{B}}\vartheta}+1]^{-1}$, with a chemical potential $\mu = \mathcal{E}_{\mathrm{F}} + (eV_{\mathrm{sd}}/2)\mathrm{sign}[v^{\alpha}_{q}(k)]$. It is displaced from its equilibrium value $\mathcal{E}_{\mathrm{F}} = 0$. We refer to $\mathcal{E}_{\mathrm{F}}$ as the common chemical potential of the whole system including both the nanotube and reservoirs. Also, ϑ refers to the temperature. For $V_{\mathrm{sd}} > 0$, right-going and left-going electrons have $\mu_{\mathrm{L}} = \mathcal{E}_{\mathrm{F}} + eV_{\mathrm{sd}}/2$ and $\mu_{\mathrm{R}} = \mathcal{E}_{\mathrm{F}} - eV_{\mathrm{sd}}/2$, respectively. At zero temperature and $V_{\mathrm{sd}} > 0$, electronic transport takes place in the energy range $\mu_{\mathrm{R}} < E < \mu_{\mathrm{L}}$ only from the left reservoir to the right. Because at zero temperature the Fermi–Dirac function moves suddenly from one to zero, it can be represented by a step function as $n_{\mathrm{F}} = \Theta[\mathcal{E}_{\mathcal{F}} - \mathcal{E}_{q}(k) - (eV_{\mathrm{sd}}/2)\mathrm{sign}[v^{\alpha}_{q}(k)]]$. The energy conservation can also be controlled by $\mathcal{E}^{\alpha}_{q}(k) = \mathcal{E}^{\alpha}_{q'}(k')$. Upon substituting the zero-temperature Fermi function into equation (19),

and after differentiating over the $V_{\rm sd}$, we obtain the following dimensionless form (scaled in atomic Rydberg units) for the DC:

$$\frac{G^{\alpha\alpha}_{\rm imp}(V_{\rm sd},\mathcal{E}_{\mathcal{F}})}{G_0}=\frac{\pi^2}{2}\sum_{q=1}^{N_t/2}\sum_{q'=1}^{N_t/2}\sum_{k\in}^{\rm FBZ}\sum_{k'\in}^{\rm FBZ}\sum_{\xi=1}^{r}\sum_{\eta=1}^{r}J^{qq'}_{\xi,\alpha\alpha}(k,k')J^{q'q}_{\eta,\alpha\alpha}(k',k)$$
$$\times\,\delta\left[\mathcal{E}^{\alpha}_{q}(k)-\mathcal{E}^{\alpha}_{q'}(k')\right]\left[{\rm sign}[v^{\alpha}_{q}(k)]{\rm sign}[v^{\alpha}_{q'}(k')]-1\right]$$
$$\times\left\{\delta\left[\mathcal{E}_{\mathcal{F}}-\mathcal{E}^{\alpha}_{q}(k)-\frac{eV_{\rm sd}}{2}{\rm sign}[v^{\alpha}_{q}(k)]\right]\right.$$
$$\left.+\,\delta\left[\mathcal{E}_{\mathcal{F}}-\mathcal{E}^{\alpha}_{q'}(k')-\frac{eV_{\rm sd}}{2}{\rm sign}[v^{\alpha}_{q'}(k')]\right]\right\}. \tag{20}$$

Similar to the current, $G^{\alpha\alpha}_{\rm total,imp}=G^{++}_{\rm imp}+G^{--}_{\rm imp}$. Equation (20), which actually gives an impurity-induced quantum correction to the conductance, is a multi-band expression embracing both intrasubband and intersubband scattering processes. It can be employed for arbitrary number of subbands and arbitrary number of impurities positioned at arbitrary locations over the tubular surface. More importantly, the expression $[{\rm sign}[v^{\alpha}_{q}(k)]{\rm sign}[v^{\alpha}_{q'}(k')]-1]$ controls the scattering event from the initial state to the final state via the sign of the electron velocity. It requires that only backward scattering events are possible in one-dimensional systems like nanotubes. This is contrary to the traditional metals for which impurities backscatter carriers through a series of small-angle scattering events. Additionally, the expression $\delta[\mathcal{E}_{\mathcal{F}}-\mathcal{E}^{\alpha}_{q}(k)-(eV_{\rm sd}/2){\rm sign}[v^{\alpha}_{q}(k)]]$ illustrates the more states around and at $\mathcal{E}_{\mathcal{F}}$, i.e. the more ways an electron can scatter to it. It is also worth noting that, using equation (20), one would consider the transition probability between two states $|q,k,\zeta\rangle$ and $|q',k',\zeta\rangle$ due to the scattering with impurities [43] (see appendix B).

Furthermore, the resistance of any material with lattice structure is determined by the impurity scattering at low temperatures and the phonons at high temperatures. This is because the Bloch wave does not result in a resistance. At zero temperature the quantum mechanical coherency becomes more important because the phase coherence length l_ϕ increases with decreasing temperature. When the coherence length l_ϕ exceeds the elastic mean free path l_m, scattering on different impurities can interfere. Other perturbations such as an Aharonov–Bohm flux or inelastic scattering events like electron–electron and electron–phonon interactions give rise to the phase breaking, and thus l_ϕ becomes finite. More remarkably, the coherent backscattering (CBS) of the electron is an effect that describes the appearance of a backscattered peak when the electron travelling in a time-reversed path self-interferes constructively in the backscattered direction. This means that the electronic wave is weakly localized. This leads to an increase in the resistance due to the quantum interference between scattering waves. The suppression of the backward scattering is ascribed to the destructive interference for any pairs of time-reversed paths; hence a negative DC value is obtained. At low temperatures the weak localization (WL) and universal conductance fluctuations (UCFs) are two important interference processes in low-dimensional mesoscopic systems [43]. More discussion on the weak localization correction to the conductance can be found in [49] and [50]. In the next section we use energy–momentum conservation requirements to evaluate equation (20) at some special k-points in the FBZ.

3. The J-function and backscattering from impurities in metallic nanotubes

In this section, we calculate the DC for armchair and zigzag nanotubes. Energy and momentum conservation requires that we need to find the solution of the equation $\mathcal{E}^{\alpha}_{q}(k)=\mathcal{E}^{\alpha}_{q'}(k+\mathbf{g})$, in

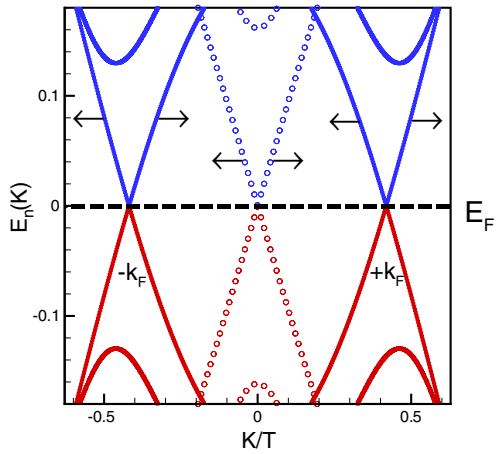

Figure 1. The energy dispersion relation for bands magnified near the Fermi level, with $E_{\rm F} = 0$. Antibonding bands (blue—$E_n(k) > 0$) are symmetric to the bonding bands (red—$E_n(k) < 0$). A two-band model consisting of the $(6, 6)$ armchair (solid line) and $(6, 0)$ zigzag (circle) nanotubes is shown. There are two modes with linear dispersion relations crossing the Fermi energy at two points $-k_{\rm F}$ and $+k_{\rm F}$. One of two modes involves electrons travelling to the right and the other electrons travelling to the left. At $V_{\rm sd} = 0$ and zero temperature all states of the valence band are occupied. The electron scattering processes change electrons from right moving to left moving, leading to electrical resistance. In general, both intrasubband and intersubband scattering events are likely. Energies are scaled in Rydbergs and lengths in bohr radius.

which **g** is the transferred momentum. It actually leads to a relation between k and **g** and may have up to four roots in the FBZ (see figure 1). Using equation (3) for the (n, n) armchair nanotubes one finds

$$\mathbf{g}^{\pm} = -k \pm \frac{2}{\sqrt{3}a_{cc}} \arccos\left\{-\frac{1}{2}\cos\left(\frac{3q'a_{cc}}{2r_t}\right) \pm \frac{1}{2}\sqrt{\cos^2\left(\frac{3q'a_{cc}}{2r_t}\right) + 4\cos^2\left(\frac{\sqrt{3}ka_{cc}}{2}\right) + 4\cos\left(\frac{\sqrt{3}ka_{cc}}{2}\right)\cos\left(\frac{3qa_{cc}}{2r_t}\right)}\right\}, \tag{21}$$

and for the $(n, 0)$ zigzag nanotubes the equivalent expression is given by

$$\mathbf{g}^{\pm} = -k \pm \frac{2}{3a_{cc}} \arccos\left\{\frac{1}{\cos(\frac{\sqrt{3}q'a_{cc}}{2r_t})}\left(-\cos^2\left(\frac{\sqrt{3}q'a_{cc}}{2r_t}\right) + \cos^2\left(\frac{\sqrt{3}qa_{cc}}{2r_t}\right) + \cos\left(\frac{\sqrt{3}qa_{cc}}{2r_t}\right)\cos\left(\frac{3ka_{cc}}{2}\right)\right)\right\}. \tag{22}$$

The energy band of metallic nanotubes can be approximated by $\mathcal{E}_q^{\alpha}(k) \simeq \alpha\gamma_0|1 - 2\cos(kT/2)|$ and $\mathcal{E}_q^{\alpha}(k) \simeq \alpha\hbar v_{\rm F}|k|$ for armchair and zigzag tubes, respectively, as long as we restrict our interest to a two-band model, i.e. a few hundred meV from $\mathcal{E}_{\rm F}$. This means that, at small applied bias voltage electrons are injected only into crossing subbands. Taking into account the nonparabolicity of the energy dispersion of the armchair-like nanotubes, we obtain two sets of bands with a linear dispersion relation intersecting at $+k_{\rm F}$ and $-k_{\rm F}$ given by $\mathcal{E}_q^{\alpha}(k) \simeq \alpha\hbar v_{\rm F}|k - k_{\rm F}|$ and $\mathcal{E}_q^{\alpha}(k) \simeq \alpha\hbar v_{\rm F}|k + k_{\rm F}|$, respectively. The Fermi velocity is defined by $v_{\rm F} = 3\gamma_0 a_{cc}/2\hbar \approx 10^6$ m s^{-1}. Furthermore, Anantram [44] has shown that for the armchair

nanotubes (n, n) at applied bias voltage larger than $(\gamma_0/e)\sin(\pi/n)$, electrons are injected into non-crossing subbands. The contribution of these electrons to the current is determined by the competing processes of Bragg reflection and Zener-type intersubband tunnelling. In this work we consider only the intrasubband scattering of electrons, i.e. $|q, k\rangle \to |q', k'\rangle = |q, k + \mathbf{g}\rangle$.

3.1. Armchair nanotubes: intrasubband scattering $(q = q')$

For the armchair tubes, equation (21) has four scattering roots as follows:

$$\begin{aligned} &\tilde{g}^{\pm} = 0, \\ &-2k, \\ &-k \pm \frac{2}{\sqrt{3}a_{cc}} \arccos\left[\cos\left(\frac{3qa_{cc}}{2r_t}\right) + \cos\left(\frac{\sqrt{3}ka_{cc}}{2}\right)\right], \end{aligned} \tag{23}$$

$k' = k$: The root $\mathbf{g}^{\pm} = 0$ means that both discrete q and continuous k quantum numbers are conserved, and we have no scattering. In this case the expression $\mathrm{sign}[v_q^{\alpha}(k)]\mathrm{sign}[v_{q'}^{\alpha}(k')]$ in equation (20) becomes $\mathrm{sign}[v_q^{\alpha}(k)]\mathrm{sign}[v_q^{\alpha}(k)]$, which is equal to unity. Thus, the DC becomes zero. In other words, we have no correction to the total conductance of the tube. Ando *et al* [23] have used the $\mathbf{k}\cdot\mathbf{p}$ approximation to treat backscattering from impurities in metallic nanotubes, and they showed that the small wavevector transfer backscattering is small. Moreover, McEuen *et al* [40] have reported experimental evidences of the lack of backscattering in metallic nanotubes compared to semiconducting ones.

$k' = -k$: The root $\mathbf{g}^{\pm} = -2k$ gives rise to the backscattering of the electron within the same subband to another Fermi point. For this case the **J**-function is given by

$$J^{q}_{\xi,\alpha\alpha}(k) = \frac{g}{2\mathcal{M}\mathcal{N}} \sum_{l} \sum_{R_j} \mathrm{e}^{-\mathrm{i}2lTk} \mathrm{e}^{-\mathrm{i}2k\left(\vec{R}_j\cdot\frac{\vec{T}}{T}\right)} \left(\delta_{\vec{x}_\xi,\vec{T}_l+\vec{R}_j+\vec{d}_1} + \delta_{\vec{x}_\xi,\vec{T}_l+\vec{R}_j+\vec{d}_2}\right), \tag{24}$$

for a *single* impurity located at $\vec{x}_\xi = \vec{T}_{l_1} + \vec{R}_{j_1} + \vec{d}_1$, equation (24) reads

$$J^{q}_{\xi,\alpha\alpha}(k) = \left(\frac{g}{2\mathcal{M}\mathcal{N}}\right) \mathrm{e}^{-\mathrm{i}2k\left[l_1T + \left(\vec{R}_{j_1}\cdot\frac{\vec{T}}{T}\right)\right]}. \tag{25}$$

The band structure and velocity are even and odd functions of k, respectively. It yields $\mathrm{sign}[v_q^{\alpha}(-k)] = -\mathrm{sign}[v_q^{\alpha}(k)]$. Thus, equation (20) can be written as follows:

$$\frac{G^{\alpha\alpha}_{\mathrm{imp}}(V_{\mathrm{sd}}, \mathcal{E}_{\mathcal{F}})}{G_0} = e|V_{\mathrm{sd}}|\left(\frac{\pi g}{2\mathcal{M}\mathcal{N}}\right)^2 \sum_{q=1}^{N_t/2} \sum_{k\in}^{\mathrm{FBZ}} \delta\left\{\left[\mathcal{E}_{\mathcal{F}} - \mathcal{E}_q^{\alpha}(k)\right]^2 - \left(\frac{eV_{\mathrm{sd}}}{2}\right)^2\right\}. \tag{26}$$

For a *couple* of impurities located at $\vec{x}_\xi = \vec{T}_{l_1} + \vec{R}_{j_1} + \vec{d}_1$ and $\vec{x}_\eta = \vec{T}_{l_2} + \vec{R}_{j_2} + \vec{d}_2$, the problem is less trivial. In this case, equation (20) can be found to be

$$\begin{aligned} \Re\left(\frac{G^{\alpha\alpha}_{\mathrm{imp}}(V_{\mathrm{sd}}, \mathcal{E}_{\mathcal{F}})}{G_0}\right) = e|V_{\mathrm{sd}}|\left(\frac{\pi g}{2\mathcal{M}\mathcal{N}}\right)^2 \sum_{q=1}^{N_t/2} \sum_{k\in}^{\mathrm{FBZ}} \delta\left\{\left[\mathcal{E}_{\mathcal{F}} - \mathcal{E}_q^{\alpha}(k)\right]^2 - \left(\frac{eV_{\mathrm{sd}}}{2}\right)^2\right\} \\ \times \cos\left\{2k\left((l_2 - l_1)T + (\vec{R}_{j_2} - \vec{R}_{j_1})\cdot\frac{\vec{T}}{T}\right)\right\}; \end{aligned} \tag{27}$$

it contains the interference term expressing the NDC. Because $\mathcal{E}_q^{+}(k) = -\mathcal{E}_q^{-}(k)$; if $\mathcal{E}_{\mathrm{F}} = 0$ then $G^{++}_{\mathrm{imp}}/G_0 = G^{--}_{\mathrm{imp}}/G_0$.

It is also interesting to point out that equation (27) clarifies the density of states (DOS) with energies $\mathcal{E}_{\mathcal{F}} = \mathcal{E}_q^{\alpha}(k) \pm (eV_{\mathrm{sd}}/2)\mathrm{sign}[v_q^{\alpha}(k)]$ but they are weighted with the interference factor. This factor represents the overlap between the Bloch state and the atomic states located at ξ and η, namely the probability that a crystal electron spends time in the electronic states at positions

ξ and η. In fact, it can be referred to as the *spectral function*. A spectral function can be defined to treat situations in which the contributions of states are weighted by their wavefunctions at the points in question. It can be considered as a generalized density of states (GDOS) given by [51]

$$\mathrm{GDOS}^{\alpha}_{\pm}(\mathcal{E}_{\mathcal{F}}, V_{\mathrm{sd}}, \vec{x}_{\xi}, \vec{x}_{\eta}) = \sum_{q=1}^{N_t/2} \sum_{k\in}^{\mathrm{FBZ}} \phi^{*,\alpha}_{q}(k, \vec{x}_{\xi}) \phi^{\alpha}_{q}(k, \vec{x}_{\eta}) \delta\left(\mathcal{E}_{\mathcal{F}} - \mathcal{E}^{\alpha}_{q}(k) \pm \frac{eV_{\mathrm{sd}}}{2} \mathrm{sign}[v^{\alpha}_{q}(k)]\right); \tag{28}$$

in the case of a single impurity the GDOS reduces to the local density of states (LDOS), written as

$$\mathrm{LDOS}^{\alpha}_{\pm}(\mathcal{E}_{\mathcal{F}}, V_{\mathrm{sd}}, \vec{x}_{\xi}) = \sum_{q=1}^{N_t/2} \sum_{k\in}^{\mathrm{FBZ}} |\phi^{\alpha}_{q}(k, \vec{x}_{\xi})|^2 \delta\left(\mathcal{E}_{\mathcal{F}} - \mathcal{E}^{\alpha}_{q}(k) \pm \frac{eV_{\mathrm{sd}}}{2} \mathrm{sign}[v^{\alpha}_{q}(k)]\right). \tag{29}$$

Comparing equations (27)–(29) manifests that the differential conductance is a measure of either the GDOS or LDOS. The LDOS is in essence the diagonal part of the GDOS. The oscillatory term in equation (27) originates from the interference between scattered waves by impurities. The amplitude of the oscillations is the product of amplitudes for an electron in the Bloch state $|q, k; \zeta\rangle$ to be in atomic orbitals $|\vec{x}_{\xi}\rangle$ and $|\vec{x}_{\eta}\rangle$, i.e. the expression $\langle \vec{x}_{\xi}|q, k; \zeta\rangle\langle \vec{x}_{\eta}|q, k; \zeta\rangle$ generates an interference pattern in both the DC and GDOS. Furthermore, using the scanning tunnelling microscopic (STM) pattern technique, the tunnelling conductance can be found to scale with the nanotube LDOS [52–54].

For simplicity, we have assumed that $R_{j_2} = R_{j_1}$, i.e. two impurities are substituted on equivalent sites AA or BB with the same circumferential angle along the tube axis. These arrangements of impurities break all mirror symmetry planes containing the tube axis [20]. Also, we assume a non-doped and non-gated tube, in which $\mathcal{E}_{\mathrm{F}} = 0$. By turning the sum over k into an integral and taking into account the linear dispersion relation, equation (27) leads to

$$\Re\left[\frac{G^{\alpha\alpha,\mathrm{arm}}_{\mathrm{imp}}(V_{\mathrm{sd}}, \mathcal{E}_{\mathcal{F}})}{G_0}\right] = \left(\frac{\pi g^2 T^{\mathrm{arm}}}{2\mathcal{M}\mathcal{N}^2_{\mathrm{arm}}}\right) \cos\left[2k_{\mathrm{F}}(l_2 - l_1)T^{\mathrm{arm}}\right] \cos\left[\left(\frac{eV_{\mathrm{sd}}}{\hbar V_{\mathrm{F}}}\right)(l_2 - l_1)T^{\mathrm{arm}}\right]. \tag{30}$$

The total DC is $\Re[G^{\mathrm{tot,arm}}_{\mathrm{imp}}/G_0] = 2\Re[G^{++,\mathrm{arm}}_{\mathrm{imp}}/G_0] = 2\Re[G^{--,\mathrm{arm}}_{\mathrm{imp}}/G_0]$. This equation shows that impurity-infected nanotubes have atomic scale characteristics in their transport properties. The key point is that the electron is elastically scattered back to a momentum directly opposite to its original momentum state in the momentum space. In other words, in the real space the electron returns to its original position. The phase memory of the electron is maintained through several scattering events in the time-reversed paths required for the weak localization. We can assume an infinite phase relaxation time. In that case, the system size plays the role of the phase-coherence length. It seems that this interference correction to the conductance could be attributed to the *zero-temperature/elastic weak-localization correction*. However, in a real nanotube the electron cannot maintain its coherency over arbitrary long distances owing to inelastic scattering events that make decoherence happen. Coupling to other degrees of freedom such as electron–electron or electron–phonon scattering events breaks the phase coherency between the time-reversed paths [43]. Suzuura *et al* [49] have used the $\mathbf{k}\cdot\mathbf{p}$ approximation to investigate the weak localization in metallic nanotubes. The most significant aspect, as a consequence of the *quantum interference correction*, is that the DC as a function of the bias voltage takes negative values. Actually, it originates from not only the QI effects but also the pseudospin conservation rule, and alters with manipulating impurities over the tubular surface. It is a direct outcome of the rotational symmetry of carbon nanotubes, and is different from the

mechanism responsible for the NDC in Esaki diodes [45, 46]. Practically, it is somewhat like that of the resonant tunnelling diode (RTD) [13, 47]. The NDC feature has a broad range of applications including logic circuit, amplification, and fast switching.
$k' = \pm(2/\sqrt{3}a_{cc})\arccos[\cos(3qa_{cc}/2r_t) + \cos(\sqrt{3}ka_{cc}/2)]$: The third and fourth roots are actually the intersubband backscattering around the same Fermi point. It is prohibited for the two crossing subbands of the armchair SWCNT by the pseudospin conservation rule [22]. Several rather surprising results can be found concerning the effects of local defects on the quantum conductance of the (n, n) metallic carbon nanotubes in [19].

3.2. Zigzag nanotubes: intrasubband scattering $(q = q')$

For the case of metallic zigzag tubes, equation (22) has two scattering roots as follows:

$$\mathbf{g}^{\pm} = 0, -2k; \tag{31}$$

the previous discussions concerning armchair nanotubes can also be followed. Moreover, it is important to remember that because the two carbon atoms A and B inside a graphite unit cell belong to two different sublattices, the impurity can occupy one of the lattice sites. The configurations of SWCNTs with two substitutional impurities can be categorized into two various classes: AA (or BB) class and AB class. As shown in equation (24), for armchair nanotubes the **J**-function is independent of whether the impurity is located at the A-site or the B-site, but it is different for the zigzag ones. In other words, for the armchair nanotubes we obtain $\Gamma^*(q/r_t, k)\Gamma(q/r_t, -k) = 1$, while for the case of metallic zigzag ones this is not equal to unity. However, we assume that impurities are placed at the B-sites. Again by turning the sum over k into an integral and taking into account the linear band structure related to the metallic zigzag nanotubes, equation (27) yields

$$\Re\left[\frac{G_{\rm imp}^{\alpha\alpha,\rm zig}(V_{\rm sd}, \mathcal{E}_{\mathcal{F}})}{G_0}\right] = \left(\frac{\pi g^2 T^{\rm zig}}{2\mathcal{M}\mathcal{N}_{zig}^2}\right)\cos\left[\left(\frac{eV_{\rm sd}}{\hbar V_{\rm F}}\right)(l_2 - l_1)T^{\rm zig}\right]; \tag{32}$$

the total DC is also $\Re[G_{\rm imp}^{\rm tot,zig}/G_0] = 2\Re[G_{\rm imp}^{++,\rm zig}/G_0] = 2\Re[G_{\rm imp}^{--,\rm zig}/G_0]$.

4. Results and discussions

The unique electrical properties of SWCNTs originates from confining the carriers over the tubular surface. It restricts the carriers to move only in two directions. Using the two-terminal Landauer–Bütticker approach for a two-band model, the whole resistance of the nanotube in the presence of scatterers is approximately given by [13, 14, 48]

$$G_{\rm tube}^{-1} = (2G_0)^{-1} + G_{\rm imp}^{-1} + G_{c1}^{-1} + G_{c2}^{-1}. \tag{33}$$

In the above equation, the first term, which results from the mismatch of the number of conducting channels in the nanotube and the macroscopic metal leads, is the resistance of a perfect ballistic nanotube with perfect contacts. In the absence of scattering events, in which transport is ballistic, the second term is negligible. The two last terms, ignored here, are owing to imperfect contacts such as those produced by interface barriers. To investigate the behaviour of the total DC as a function of $V_{\rm sd}$, we have numerically calculated equations (30) and (32) for armchair and zigzag nanotubes, respectively. As expected, the results are the same for both repulsive and attractive impurity potentials. Let us suppose $eV_{\rm sd} \in [-0.035, 0.035]$, $g = 10^3\gamma_0$ representing a typical impurity, and $\mathcal{M} = 1000\,000$. In equation (30), the product of two cosine terms is actually a resultant wave originating from the superposition of two standing waves with the same amplitude but different wavenumbers $\mathbf{k} \equiv eV_{\rm sd}/2\hbar V_{\rm F} + k_{\rm F}$

and $\mathbf{k}' \equiv eV_{\rm sd}/2\hbar V_{\rm F} - k_{\rm F}$. These two initial standing waves describing two degenerate quasi-bound states (or resonant states in the case of metallic nanotubes) induced by impurities in the FBZ are $f = (\pi T g^2/4\mathcal{M}\mathcal{N}^2)\cos[2\mathbf{k}(l_2 - l_1)T]$ and $f' = (\pi T g^2/4\mathcal{M}\mathcal{N}^2)\cos[2\mathbf{k}'(l_2 - l_1)T]$. Both f and f' have even parity and essentially give rise to the same interference pattern for both positive and negative values of wavenumbers. When they are in phase, constructive interference occurs, while destructive interference occurs where they are out of phase. As can be seen from figure 1, we can consider two equivalent possible types of interference near the Fermi energy: (1) intra-branch interference where both $\mathbf{k}$ and $\mathbf{k}'$ remain in the same branch; (2) interbranch interference where they are in branches with opposite velocities. This can be interpreted as follow. The π and π^* energy bands are orthogonal in the impurity-free nanotubes, while in the impurity-infected ones they can mix. It should be pointed out that a single impurity or two impurities positioned at equivalent sites break all mirror symmetry planes containing the tube axis [19, 20]. However, in our model, owing to the conservation of the pseudospinor, only intra-branch and interbranch interference phenomena within the same subband are allowed. As an another important outcome, a comparison between equations (30) and (32) reveals that for the zigzag nanotubes two waves f and f' are always in phase and interfere constructively in such a way that the resultant wave has twice the amplitude of the individual waves, while for the armchair nanotubes they interfere both constructively and destructively. One can actually understand this as being due to the difference in their electronic band structure. In equation (30), let us define $Q \equiv eV_{\rm sd}/\hbar v_{\rm F}$ and $(l_2 - l_1)T \equiv l_m$ (the elastic mean free path). The positions of the nth node of the DC, in which the amplitude of the resultant wave is equal to zero, is then given by $Q_n = (2n+1)\pi/2l_m$, with $n = 0, \pm1, \pm2, \ldots$. On the other hand, at the antinode points the amplitude of the resultant wave has its maximum value. The period of oscillations determining peak splitting in the Q-space can be found to be $\varpi = 3\pi a_{cc}/l_m$. For armchair nanotubes the Fermi wavelength is determined by $\lambda_{\rm F} = 3T$, while it is infinity for the zigzag ones.

For a single impurity, we have $l_2 = l_1$. Evaluating equations (30) and (32) leads to a constant value of the DC within the chosen energy window. The impurity potential virtually affects the DC by scattering incoming electrons whose energies are around the Fermi energy, and it traps electrons due to the existence of resonant backscattering from quasi-bound states. We can see, for example, that for a (6, 6) tube with $\mathcal{N} = 12$ and a (12, 12) tube with $\mathcal{N} = 24$ the DC is about 0.4976 and 0.1244, respectively. Also, for the (6, 0) and (12, 0) zigzag nanotubes, the DC is about 0.4308 and 0.1077, respectively. As a result, an increase in the tube radius corresponds to a change from quasi-one-dimensional to two-dimensional behaviour. This means that the (12, 12) and (12, 0) nanotubes have a bigger number of atoms around their circumferences, so raising the number of paths by which the electron can travel around the impurity and decreasing the DC. Another consequence is that, due to the difference in the geometrical symmetry, the DC of the (6, 6) nanotube of radius $r_t \simeq 7.79$ bohr is bigger than that of the (6, 0) nanotube of radius $r_t \simeq 4.49$ bohr. Furthermore, comparing equations (29) and (30) yields that this non-zero amount of the DC can be interpreted in terms of the LDOS near the location of the impurity.

Figure 2 depicts several results coming from evaluating equations (30) and (32) for the DC as a function of l_m/a_{cc}. Panel (a) shows the calculated DC for the (6, 6) and (12, 12) nanotubes with $eV_{\rm sd} = 0.09\gamma_0$. In panel (b) the curve is repeated for the noted tubes with $eV_{\rm sd} = 0.05\gamma_0$. In both cases, due to adding two waves with the same amplitude but different wavenumbers, beating occurs. The resultant waveform can be thought of as a wave with wavenumber $k_{\rm ave}^{\rm arm} = (\mathbf{k} + \mathbf{k}')/2 = eV_{\rm sd}/2\hbar V_{\rm F}$ which is constrained by an envelope with a wavenumber $k_{\rm beat}^{\rm arm} = |\mathbf{k} - \mathbf{k}'| = 2k_{\rm F}$. Panel (c) exhibits the calculated DC as a function of l_m/a_{cc} for the (6, 0) and (12, 0) nanotubes, with $eV_{\rm sd} = 0.09\gamma_0$. As expected, for zigzag nanotubes

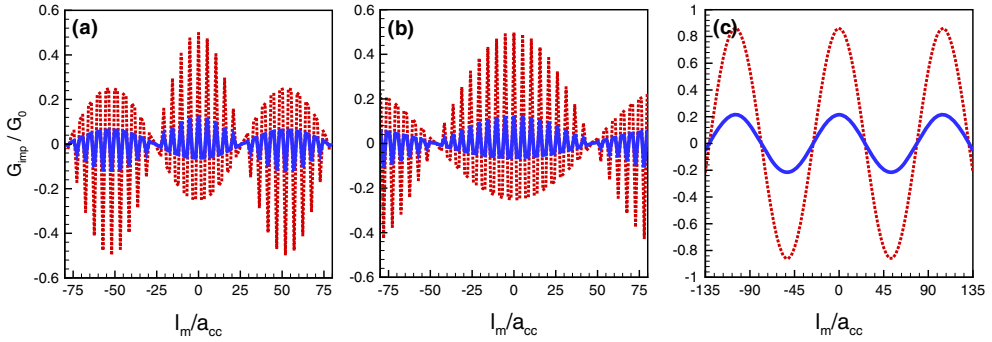

Figure 2. Calculated results as a function of l_m/a_{cc} for the armchair and zigzag nanotubes with two impurities: (a) $G_{\rm imp}/G_0$ is plotted for the (6, 6) (dotted—red line) and (12, 12) (solid—blue line) nanotubes for $eV_{\rm sd} = 0.09\gamma_0$, with $\mathbf{k} \simeq \pm 0.4556$ and $\mathbf{k}' \simeq \pm 0.4335$; (b) $G_{\rm imp}/G_0$ is plotted for the (6, 6) (dotted—red line) and (12, 12) (solid—blue line) nanotubes for $eV_{\rm sd} = 0.05\gamma_0$, with $\mathbf{k} \simeq \pm 0.4507$ and $\mathbf{k}' \simeq \pm 0.4384$. (c) $G_{\rm imp}/G_0$ is plotted for the (6, 0) (dotted—red line) and (12, 0) (solid—blue line) metallic zigzag nanotubes for $eV_{\rm sd} = 0.09\gamma_0$, with $\mathbf{k} = \mathbf{k}' \simeq \pm 0.011\,03$. No envelope function describing slow oscillations can be found in the case of zigzag tubes. Notice that for the armchair nanotubes $k_{\rm F} = 2\pi/3T \simeq 0.4445$, while for the zigzag ones $k_{\rm F} = 0$.

$k_{\rm ave}^{\rm zig} = k_{\rm ave}^{\rm arm}$, but $k_{\rm beat}^{\rm zig} = 0$. The plots are quite different between the armchair and zigzag tubes: the slowly oscillating envelope of the fast oscillations is clarified in panels (a) and (b), but only fast oscillations in panel (c). Both slow and fast oscillations illustrate characteristics shared by all armchair SWCNTs. One can obtain the period of slow oscillations for armchair tubes in real space as $\tau_{\rm slow} = \lambda_{\rm F}/2$. Moreover, the squared standing waves can be used to measure the density of states imaged by the STM experiment, which is sensitive to the square of the wavefunction [52–54].

Figure 3 shows the calculated DC as a function of the normalized source–drain energy for the (6, 6) nanotubes with two impurities substituted on equivalent sublattices within the same hexagonal unit cell, but at different nanotube unit cells. It is obvious that the DC does not alter in a monotonic way; instead it exhibits oscillations with a certain period. The period of oscillations is directly proportional to the reciprocal of l_m. It is given by $\varpi = \pi\sqrt{3}/(l_2 - l_1)$ because for the armchair nanotubes $T^{\rm arm} = \sqrt{3}a_{cc}$. The more important aspect is that the maximal amplitude for the DC is obtained wherever $l_m/\lambda_{\rm F} = 3n$, with n integer. They correspond to the antinodes in the DC curve. $G_{\rm imp}/G_0$ as a function of $eV_{\rm sd}/\gamma_0$ is plotted for $l_m = T^{\rm arm}$ in figure 3(a). For this value of l_m we obtain $\varpi = \pi\sqrt{3}$, and the DC does not represent remarkable oscillations. In figure 3(b), the DC is depicted for $l_m = 50T^{\rm arm}$, with $\varpi = \pi\sqrt{3}/50$, and it exhibits quite visible oscillations. Two typical very fast oscillations in the DC behaviour are described in figures 3(c) and (d) for $l_m = 1000T^{\rm arm}$ and $l_m = 2499T^{\rm arm}$, respectively. In both cases $l_m \gg a_{cc}$, and their periods are $\varpi = \pi\sqrt{3}/1000$ and $\varpi = \pi\sqrt{3}/2499$, respectively. As already mentioned, no quantum interference occurs between different channels in π and π^* bands. We expect that, in case someone considers intersubband scattering processes as well as intrasubband ones, due to interference phenomena between various subbands fast oscillations may be modulated by slow ones. Additionally, a change in the interference pattern can be followed by altering the tube size. As in the case of the single-impurity problem, an increase in the tube radius raises the number of graphene unit cells over the tubular surface by the factor $\mathcal{N}$. Thus, the DC decreases via $1/\mathcal{N}^2$.

Figure 4 depicts the DC oscillations, which vary periodically on increasing the source–drain energy, for the (6, 0) nanotubes with two impurities located at BB sublattices within the same hexagonal unit cell, but at different nanotube unit cells. The general features follow the

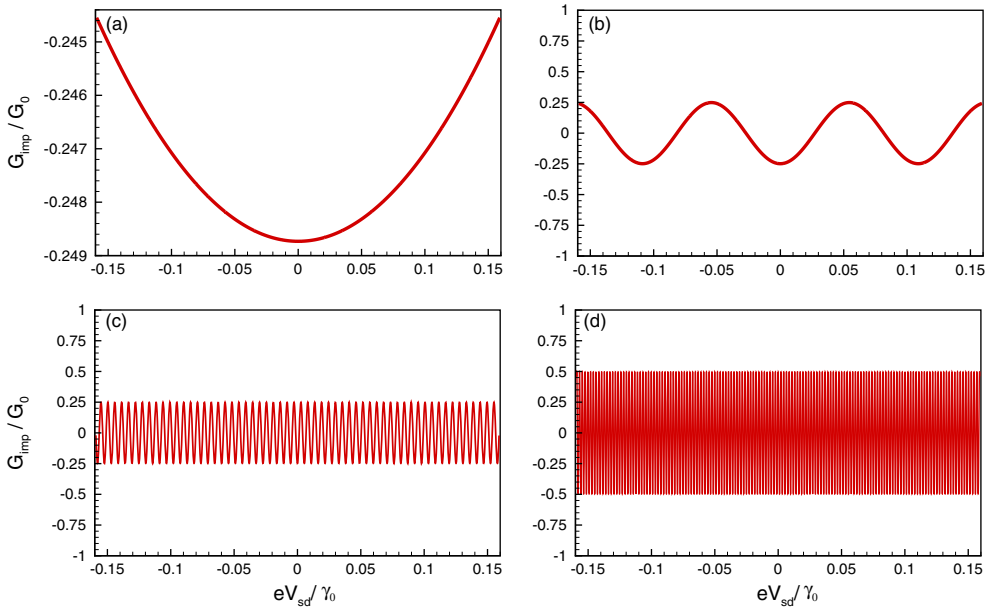

Figure 3. Calculated results, from equation (30), as a function of $eV_{\rm sd}/\gamma_0$ for $(6, 6)$ armchair nanotubes with two impurities: (a) $l_2 - l_1 = 1$, with the pick splitting $\varpi = \pi\sqrt{3}$; (b) $l_2 - l_1 = 50$, with the pick splitting $\varpi = \pi\sqrt{3}/50$; (c) $l_2 - l_1 = 1000$, with the pick splitting $\varpi = \pi\sqrt{3}/1000$; (d) $l_2 - l_1 = 2499$, with the pick splitting $\varpi = \pi\sqrt{3}/2499$. Notice that the pick splitting comes from the period of oscillations.

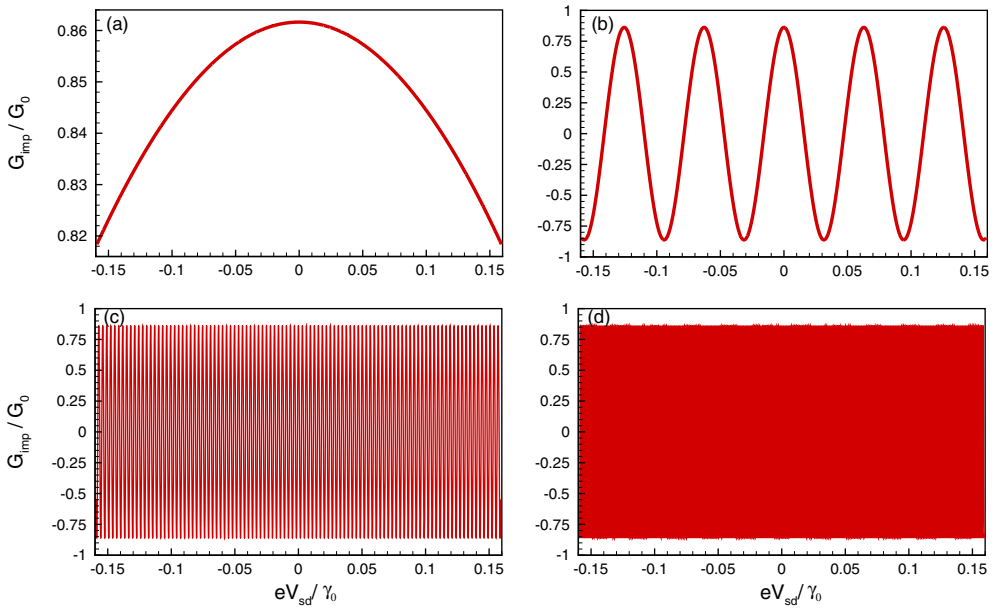

Figure 4. Calculated results, from equation (32), as a function of $eV_{\rm sd}/\gamma_0$ for $(6, 0)$ metallic zigzag nanotubes with two impurities: (a) $l_2 - l_1 = 1$, with the pick splitting $\varpi = \pi$; (b) $l_2 - l_1 = 50$, with the pick splitting $\varpi = \pi/50$; (c) $l_2 - l_1 = 1000$, with the pick splitting $\varpi = \pi/1000$; (d) $l_2 - l_1 = 2499$, with the pick splitting $\varpi = \pi/2499$.

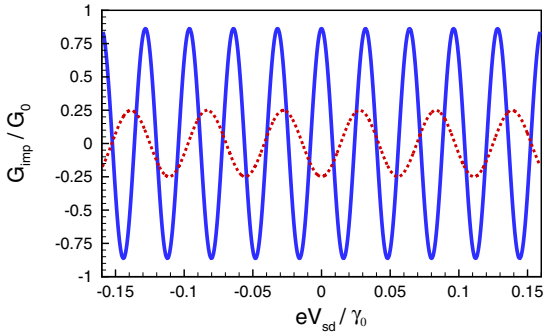

Figure 5. Calculated results, from comparing equations (30) and (32), as a function of $eV_{\rm sd}/\gamma_0$ for (6, 6) armchair (red—dotted) and (6, 0) zigzag (blue—solid) nanotubes with two impurities configured for $l_2 - l_1 = 98$. The pick splitting ratio is $\varpi^{\rm arm}/\varpi^{\rm zig} = \sqrt{3}$.

aforementioned results concerning the armchair nanotubes, but one subtle difference should be emphasized. In metallic zigzag nanotubes $T^{\rm zig} = 3a_{cc}$; therefore, the period of oscillations is given by $\varpi = \pi/(l_2 - l_1)$. In figure 4(a), $G_{\rm imp}/G_0$ as a function of $eV_{\rm sd}/\gamma_0$ is plotted when $l_m = T^{\rm zig}$. For this interdistance of impurities we find $\varpi = \pi$, and the DC exhibits no significant oscillations. Figure 4(b) shows fast oscillations for the parameter $l_m = 50T^{\rm zig}$, with $\varpi = \pi/50$. From figures 4(c) and (d) it can be seen when two impurities are very distant a very fast oscillatory behaviour appears. They correspond to $l_m = 1000T^{\rm zig}$ and $l_m = 2499T^{\rm zig}$, with $\varpi = \pi/1000$ and $\varpi = \pi/2499$, respectively.

In figure 5 the calculated DC as a function of the normalized source–drain energy for the (6, 6) armchair and (6, 0) zigzag nanotubes has been compared. $G_{\rm imp}/G_0$ as a function of $eV_{\rm sd}/\gamma_0$ is plotted when $l_2 - l_1 = 98$. The essential point is that the splitting pick ratio is always equal to $\varpi^{\rm arm}/\varpi^{\rm zig} = \sqrt{3}$. In other words, the DC of zigzag nanotubes oscillates more quickly than that of the armchair ones, i.e. $\varpi^{\rm arm} > \varpi^{\rm zig}$. More importantly, because of the constructive interference, the amplitude of periodic oscillations in the metallic zigzag nanotubes is always higher than that of the armchair ones. As a result, the *faster/higher* and *slower/shorter* oscillations can then effectively be achieved by *metallic zigzag* and *armchair* nanotubes, respectively. From this comparison it seems that the metallic zigzag nanotubes may be more suitable candidates for interference nanodevices based on metallic nanotubes.

Finally, it can be inferred that the mechanism of quantum interference between electronic waves scattered by defects memorializes a Fabry–Perot electron resonator based on metallic nanotubes. It is also worth noting that our model is flexible enough to incorporate additional scattering potentials into the Hamiltonian. For example, as the temperature of the tube is raised, the amount of electron–electron and electron–phonon scattering increases because of an increased phase space for scattering and an increase number of phonons. Therefore, the coherence length for the electron diminishes. We expect a drastic change in the interference pattern upon incorporating additional corrections related to inelastic scattering events into the DC. For example, an Aharonov–Bohm flux can bring the interference pattern under control using an additional Berry's phase [43]. Moreover, in the case of incoherent events we of course take care with the use of equation (33) [13, 14].

5. Conclusion

In summary, within the framework of a nearest-neighbour tight-binding model and by employing a method based on the energy loss for electrons travelling through the nanotube, the influence of point-like impurities on the differential conductance of infinite metallic single-wall

carbon nanotubes has been investigated. We have shown that the differential conductance of the impurity-infected MSWCNTs oscillates, and it is tunable by both the locations of impurities over the tubular surface and the axial electric field. For the case of two impurities the differential conductance exhibits periodic oscillations including both positive and negative values, while it remains constant in the case of a single impurity. We attribute this phenomenon to the intrinsic quantum interference effects. Such a result may be applied for manipulating defective metallic nanotubes into quantum interference devices. In particular, the negative differential conductance, resulting from the rotational symmetry selection-rule and quantum interference, is an unusual transport property giving rise to new atomic-scale switches, amplifiers, and memory devices.

Acknowledgments

MB is indebted to Dr Farshad Ebrahimi for bringing to his attention the problem of quantum transport and for very fruitful discussions. We also acknowledge Dr Hidekatsu Suzuura for a valuable discussion.

Appendix A. Derivation of equation (19)

The charge current of an electron scattered by impurities given by equation (19) is derived in detail. In equation (17) we define the operator $\hat{\mathcal{O}}_1(t) = [\hat{\mathcal{H}}_{\rm sd}(t), \hat{\mathcal{H}}_{\rm imp}(t)]$ as follows:

$$\hat{\mathcal{O}}_1(t) = \frac{eV_{\rm sd}}{2} \sum_{\alpha=\pm} \sum_{q,q_1,q_2=1}^{N_t/2} \sum_{k,k_1,k_2\in}^{\rm FBZ} J^{q_1q_2}_{\xi,\alpha\alpha}(k_1,k_2)\,{\rm sign}[v^\alpha_q(k)] \times \left[\hat{C}^{\dagger\alpha}_q(k,t)\hat{C}^\alpha_q(k,t),\, \hat{C}^{\dagger\alpha}_{q_1}(k_1,t)\hat{C}^\alpha_{q_2}(k_2,t)\right]. \tag{A.1}$$

Using the anti-commutation relation between Fermionic operators, the operator $\hat{\mathcal{O}}_1(t)$ can be found to be

$$\hat{\mathcal{O}}_1(t) = \frac{eV_{\rm sd}}{2} \sum_{\alpha=\pm} \sum_{q_1,q_2=1}^{N_t/2} \sum_{k_1,k_2\in}^{\rm FBZ} \sum_{\xi=1}^{r} J^{q_1q_2}_{\xi,\alpha\alpha}(k_1,k_2)\left[{\rm sign}[v^\alpha_{q_1}(k_1)] - {\rm sign}[v^\alpha_{q_2}(k_2)]\right] \times \hat{C}^{\dagger\alpha}_{q_1}(k_1,t)\hat{C}^\alpha_{q_2}(k_2,t). \tag{A.2}$$

Now, by defining the operator $\hat{\mathcal{O}}_2(t,t_1) = [\hat{\mathcal{O}}_1(t), \hat{\mathcal{H}}_{\rm imp}(t_1)]$, and taking its average, one obtains

$$\langle\hat{\mathcal{O}}_2(t,t_1)\rangle = \frac{eV_{\rm sd}}{2} \sum_{\alpha=\pm} \sum_{q_1,q_1'=1}^{N_t/2} \sum_{q_2,q_2'=1}^{N_t/2} \sum_{k_1,k_1'\in}^{\rm FBZ} \sum_{k_2,k_2'\in}^{\rm FBZ} \sum_{\xi,\eta=1}^{r} J^{q_1q_2}_{\xi,\alpha\alpha}(k_1,k_2) J^{q_2q_1}_{\eta,\alpha\alpha}(k_2,k_1) \times \left[{\rm sign}[v^\alpha_{q_1}(k_1)] - {\rm sign}[v^\alpha_{q_2}(k_2)]\right] \times \left\langle\left[\hat{C}^{\dagger\alpha}_{q_1}(k_1,t)\hat{C}^\alpha_{q_2}(k_2,t),\, \hat{C}^{\dagger\alpha}_{q_1'}(k_1',t)\hat{C}^\alpha_{q_2'}(k_2',t)\right]\right\rangle. \tag{A.3}$$

By employing Wick's theorem applied to the bracket of electron operators, we find

$$\left\langle\left[\hat{C}^{\dagger\alpha}_{q_1}(k_1,t)\hat{C}^\alpha_{q_2}(k_2,t) - \hat{C}^{\dagger\alpha}_{q_1'}(k_1',t)\hat{C}^\alpha_{q_2'}(k_2',t)\right]\right\rangle = G_0^{<,\alpha}(q_1,k_1,t;q_2',k_2',t_1)G_0^{>,\alpha}(q_2,k_2,t;q_1',k_1',t_1) - G_0^{<,\alpha}(q_1',k_1',t_1;q_2,k_2,t)G_0^{>,\alpha}(q_2',k_2',t_1;q_1,k_1,t), \tag{A.4}$$

where $G_0^<$ and $G_0^>$ are the corresponding lesser and greater single-particle Green's function of the Hamiltonian $\hat{\mathcal{H}}_{\rm tube}$ in $\vec{k} = (q/r_t, k)$ space, respectively. They are defined as follows:

$$
\begin{aligned}
G_0^{<,\alpha}(q_1,k_1,t;q_2',k_2',t_1) &= \mathrm{i}\left\langle \hat{C}^{\dagger\alpha}_{q_1}(k_1,t)\hat{C}^{\alpha}_{q_2'}(k_2',t_1)\right\rangle \\
G_0^{>,\alpha}(q_2,k_2,t;q_1',k_1',t_1) &= -\mathrm{i}\left\langle \hat{C}^{\alpha}_{q_2}(k_2,t)\hat{C}^{\dagger\alpha}_{q_1'}(k_1',t_1)\right\rangle \\
G_0^{<,\alpha}(q_1',k_1',t_1;q_2,k_2,t) &= \mathrm{i}\left\langle \hat{C}^{\dagger\alpha}_{q_1'}(k_1',t_1)\hat{C}^{\alpha}_{q_2}(k_2,t)\right\rangle \\
G_0^{>,\alpha}(q_2',k_2',t_1;q_1,k_1,t) &= -\mathrm{i}\left\langle \hat{C}^{\alpha}_{q_2'}(k_2',t_1)\hat{C}^{\dagger\alpha}_{q_1}(k_1,t)\right\rangle.
\end{aligned}
\tag{A.5}
$$

Because the Hamiltonian $\hat{\mathcal{H}}_{\mathrm{tube}}$ is diagonal in the quantum number $\vec{k}$, so is the Green's function, and therefore

$$
G_0^{<,\alpha}(q,k,t;q',k',t') = \delta_{qq'}\delta_{kk'}G_0^{<,\alpha}(q,k,;t,t'). \tag{A.6}
$$

Equation (A.5) can then be written as follows:

$$
\begin{aligned}
G_0^{<,\alpha}(q_1,k_1;t,t_1) &= \mathrm{i}n_{\mathrm{F}}\left[\mathcal{E}^{\alpha}_{q_1}(k_1)\right]\mathrm{e}^{-\mathrm{i}\mathcal{E}^{\alpha}_{q_1}(k_1)(t_1-t)} \\
G_0^{>,\alpha}(q_2,k_2;t,t_1) &= -\mathrm{i}\left[1-n_{\mathrm{F}}[\mathcal{E}^{\alpha}_{q_2}(k_2)]\right]\mathrm{e}^{-\mathrm{i}\mathcal{E}^{\alpha}_{q_2}(k_2)(t-t_1)} \\
G_0^{<,\alpha}(q_1',k_1';t_1,t) &= \mathrm{i}n_{\mathrm{F}}\left[\mathcal{E}^{\alpha}_{q_1'}(k_1')\right]\mathrm{e}^{-\mathrm{i}\mathcal{E}^{\alpha}_{q_1'}(k_1')(t-t_1)} \\
G_0^{>,\alpha}(q_2',k_2';t_1,t) &= -\mathrm{i}\left[1-n_{\mathrm{F}}[\mathcal{E}^{\alpha}_{q_2'}(k_2')]\right]\mathrm{e}^{-\mathrm{i}\mathcal{E}^{\alpha}_{q_2'}(k_2')(t_1-t)}.
\end{aligned}
\tag{A.7}
$$

We of course have $\langle \hat{C}^{\dagger\alpha}_{q}(k)\hat{C}^{\alpha}_{q}(k)\rangle = n_{\mathrm{F}}[\mathcal{E}^{\alpha}_{q}(k) + (eV_{\mathrm{sd}}/2)\mathrm{sign}[v^{\alpha}_{q}(k)]]$, where n_{F} is the Fermi–Dirac distribution function. Upon substituting equation (A.7) instead of the bracket into equation (A.3) and taking a temporal Fourier transformation, the expression of equation (19) is obtained [43].

Appendix B. The transition amplitude

To explain how our formalism can be related to Fermi's golden rule, we follow an electron after it has been scattered to a state with momentum $\vec{k}' = (q',k')$ by an impurity positioned at $\vec{x}_\mu$. When the electron hits the next impurity located at $\vec{x}_\nu$, it has acquired a phase factor $\mathrm{e}^{\mathrm{i}\Phi} = \mathrm{e}^{\mathrm{i}\vec{k}.(\vec{x}_\mu-\vec{x}_\nu)}$. Terms illustrating interference between the two scattering events will thus contain this phase factor. In equation (20), it is served by the factor $J^{qq'}_{\mu,\alpha\alpha}(k,k')J^{q'q}_{\nu,\alpha\alpha}(k',k) = \langle\alpha,q,k|\vec{x}_\mu\rangle\langle\vec{x}_\mu|q',k',\alpha\rangle\langle\alpha,q',k'|\vec{x}_\nu\rangle\langle\vec{x}_\nu|q,k,\alpha\rangle$. We rearrange this factor as $[\langle\vec{x}_\nu|q,k,\alpha\rangle\langle\alpha,q,k|\vec{x}_\mu\rangle][\langle\vec{x}_\mu|q',k',\alpha\rangle\langle\alpha,q',k'|\vec{x}_\nu\rangle]$, where the first and second brackets are the acquired phase for the electron when it is in the states $|\vec{k},\alpha\rangle$ and $|\vec{k}',\alpha\rangle$, respectively. This factor is proportional to $\mathrm{e}^{\mathrm{i}(\vec{k}-\vec{k}').(\vec{x}_\nu-\vec{x}_\mu)}$. This phase factor is equal to zero if impurities are randomly distributed. The relative phase determines whether the contributions from the four amplitudes interfere constructively or destructively. As shown, this yields resonances in the electron transport. It should also be pointed out that quantum effects such as interference between scattering on different impurities cannot be incorporated within the Born approximation scheme [43]. Moreover, the expressions $J^{qq'}_{\nu,\alpha\alpha}(k,k')$ and $J^{qq'}_{\mu,\alpha\alpha}(k,k')$ explain the partial transition amplitudes owing to impurities located at $\vec{x}_\nu$ and $\vec{x}_\mu$, respectively. Because the scattering events are independent, the probability of two or more events occurring in sequence can be found by computing the probability of each event separately, and then multiplying the results together. The expression of equation (20) contains the Cauchy product of two complex series embracing the scattering amplitudes. Thus, the double sum is actually a discrete convolution, and it can be written in terms of a single finite series as follows:

$$
\begin{aligned}
\sum_{\xi=1}^{r}\sum_{\eta=1}^{r}J^{qq'}_{\xi,\alpha\alpha}(k,k')J^{qq',*}_{\eta,\alpha\alpha}(k,k') &= \left(\sum_{\xi=1}^{r}J^{qq'}_{\xi,\alpha\alpha}(k,k')\right)\left(\sum_{\eta=1}^{r}J^{qq',*}_{\eta,\alpha\alpha}(k,k')\right), \\
&= \sum_{\nu=1}^{r}\Xi^{qq'}_{\nu,\alpha\alpha}(k,k'),
\end{aligned}
\tag{B.1}
$$

where

$$\Xi^{qq'}_{v,\alpha\alpha}(k,k') = \sum_{u=1}^{v} J^{qq'}_{u,\alpha\alpha}(k,k') J^{qq',*}_{v-u+1,\alpha\alpha}(k,k'). \tag{B.2}$$

This approach provides a vivid and generalized representation containing all diagonal (non-crossing) and off-diagonal (crossing-interference) terms of the scattering of an electron by impurities. For instance, for a single impurity, with $r = 1$, one would obtain $\Xi^{qq'}_{1,\alpha\alpha} = J^{qq'}_{1,\alpha\alpha}(k,k')J^{qq',*}_{1,\alpha\alpha}(k,k') = |J^{qq'}_{1,\alpha\alpha}(k,k')|^2$. Similarly, for a pair of impurities, with $r = 2$, and for a triplet case, with $r = 3$, one would acquire, respectively,

$$\begin{aligned}\Xi^{qq'}_{2,\alpha\alpha}(k,k') &= J^{qq'}_{1,\alpha\alpha}(k,k')J^{qq',*}_{2,\alpha\alpha}(k,k') + J^{qq'}_{2,\alpha\alpha}(k,k')J^{qq',*}_{1,\alpha\alpha}(k,k') \\ &= 2\Re\left(J^{qq'}_{1,\alpha\alpha}(k,k')J^{qq',*}_{2,\alpha\alpha}(k,k')\right),\end{aligned} \tag{B.3}$$

$$\Xi^{qq'}_{3,\alpha\alpha}(k,k') = |J^{qq'}_{2,\alpha\alpha}(k,k')|^2 + 2\Re\left(J^{qq'}_{1,\alpha\alpha}(k,k')J^{qq',*}_{3,\alpha\alpha}(k,k')\right). \tag{B.4}$$

Note that all the Ξ are quadratic in J. Thus, the total Ξ up to the third term can be written as follows:

$$\begin{aligned}\Xi_1 + \Xi_2 + \Xi_3 = {} & |J^{qq'}_{1,\alpha\alpha}(k,k')|^2 + |J^{qq'}_{2,\alpha\alpha}(k,k')|^2 + 2\Re\left(J^{qq'}_{1,\alpha\alpha}(k,k')J^{qq',*}_{2,\alpha\alpha}(k,k')\right) \\ & + 2\Re\left(J^{qq'}_{1,\alpha\alpha}(k,k')J^{qq',*}_{3,\alpha\alpha}(k,k')\right).\end{aligned} \tag{B.5}$$

The nth term, i.e. $\Xi^{qq'}_{n,\alpha\alpha}(k,k')$, has n pairs $J_u J^*_v$; for all pairs the condition $u + v = n + 1$ is satisfied. Therefore, the total transition probability of the elastic scattering from state $|q,k\rangle$ to state $|q',k'\rangle$ as a summation of partial probabilities including both diagonal and off-diagonal terms can be defined as follows:

$$W_{|q,k\rangle\longrightarrow|q',k'\rangle} = \frac{2\pi}{\hbar}\sum_{v=1}^{r}\Xi^{qq'}_{v,\alpha\alpha}(k,k')\delta\left[\mathcal{E}^{\alpha}_{q}(k) - \mathcal{E}^{\alpha}_{q'}(k')\right]\left[\mathrm{sign}[v^{\alpha}_{q}(k)]\mathrm{sign}[v^{\alpha}_{q'}(k')] - 1\right]. \tag{B.6}$$

The expression (B.6) may be considered as a generalization to Fermi's golden rule by including off-diagonal terms representing the QI. For an electron with momentum k in subband q, the elastic lifetime due to the impurity scattering can be found to be

$$\tau_q^{-1}(k) = \sum_{q'=1}^{N_t/2}\sum_{k'\in}^{\mathrm{FBZ}} W_{|q,k\rangle\longrightarrow|q',k'\rangle}. \tag{B.7}$$

This result states that the scattering rate for the electron is proportional to the density of states. The more final states that are available, the higher the scattering rate. Thus, the DC reads

$$\frac{G^{\alpha\alpha}_{\mathrm{imp}}(V_{\mathrm{sd}},\mathcal{E}_{\mathcal{F}})}{G_0} = \frac{h}{4}\sum_{q=1}^{N_t/2}\sum_{k\in}^{\mathrm{FBZ}}\tau_q^{-1}(k)\delta\left[\mathcal{E}_{\mathcal{F}} - \mathcal{E}^{\alpha}_{q}(k) - \frac{eV_{\mathrm{sd}}}{2}\mathrm{sign}[v^{\alpha}_{q}(k)]\right]. \tag{B.8}$$

It seems that the above equation could clarify how the DC is related to the elastic lifetime. More descriptions on using the golden rule in disordered tubes can be found in [6].

References

[1] Iijima S 1991 *Nature* **354** 56

[2] Saito R, Dresslhuas G and Dresslhuas M S 1998 *Physical Properties of Carbon Nanotubes* (London: Imperial College Press)

[3] Saito R, Fujita M, Dresslhuas G and Dresslhuas M S 1992 *Appl. Phys. Lett.* **60** 2204

[4] Mintmire J W, Dunlap B I and White C T 1992 *Phys. Rev. Lett.* **68** 631

[5] Hamada N, Sawada S I and Oshiyama A 1992 *Phys. Rev. Lett.* **68** 1579

[6] White C T and Todorov T N 1998 *Nature* **393** 240
[7] Tans S, Verschueren A R M and Dekker C 1998 *Nature* **393** 49
Tans S, Devoret M H, Dai H, Thess A, Smalley R E, Geerligs L J and Dekker C 1997 *Nature* **386** 474
Bockrath M, Cobden D H, McEuen P L, Chopra N G, Zettl A, Thess A and Smalley R E 1997 *Science* **275** 1922
Nygard J, Cobden D H, Bockrath M, McEuen P L and Lindelof P E 1999 *Appl. Phys.* A **69** 297
[8] Martel R, Schmidt T, Shea R H, Hertel T and Avouris Ph 1998 *Appl. Phys. Lett.* **73** 2447
[9] Soh H T, Quate C F, Morpurgo A F, Marcus C M, Kong J and Dai H 1999 *Appl. Phys. Lett.* **75** 627
[10] Javey A, Guo J, Wang Q, Lundstrom M and Dai H 2003 *Nature* **424** 654
[11] Avouris Ph 2002 *Chem. Phys.* **281** 429
[12] Landauer R 1970 *Phil. Mag.* **21** 863
[13] Datta S 1995 *Electronic Transport in Mesoscopic Systems* (Cambridge: Cambridge University Press)
[14] Imry Y 1997 *Introduction to Mesoscopic Physics* (New York: Oxford University Press)
[15] Orlikowski D, Mehrez H, Taylor J, Guo H, Wang J and Roland C 2001 *Phys. Rev.* B **63** 155412
[16] Frank S, Poncharal P, Wang Z L and de Heer W A 1998 *Science* **280** 1744
[17] Nardelli M B 1999 *Phys. Rev.* B **60** 7828
Nardelli M B and Bernholc J 1999 *Phys. Rev.* B **60** 16338
[18] Chico L, Benedict L X, Louie S G and Cohen M L 1996 *Phys. Rev.* B **54** 2600
[19] Choi H J, Ihm J, Louie S G and Cohen M L 2000 *Phys. Rev. Lett.* **84** 2917
[20] Song H-F, Zhu J-L and Xiong J-J 2002 *Phys. Rev.* B **65** 085408
[21] Anantram M P and Govindan T R 1998 *Phys. Rev.* B **58** 4882
[22] Petrov A G and Rotkin S V 2004 *Phys. Rev.* B **70** 035408
[23] Ando T and Nakanishi T 1998 *J. Phys. Soc. Japan* **67** 1704
Ando T, Nakanishi T and Saito R 1998 *J. Phys. Soc. Japan* **67** 2857
[24] Roche S, Triozon F and Rubio A 2001 *Appl. Phys. Lett.* **79** 3690
[25] Liu Y and Guo H 2004 *Phys. Rev.* B **69** 115401
[26] Lee R S, Kim H J, Fischer J E, Thess A and Smalley R 1997 *Nature* **388** 255
[27] Yao Z, Postma H W Ch, Balents L and Dekker C 1999 *Nature* **402** 273
[28] Bockrath M, Liang W, Bozovic D, Hafner J H, Lieber C H, Tinkham M and Park H 2001 *Science* **291** 283
[29] Collins P G, Zettl A, Bando H, Thess A and Smalley R E 1997 *Science* **278** 100
[30] Stone A J and Wales D J 1986 *Chem. Phys. Lett.* **128** 501
[31] Namiranian A 2004 *Phys. Rev.* B **70** 073402
[32] Kulik I O 1967 *JETP Lett.* **5** 345
[33] Kulik I O, Omelyanchouk A N and Tuluzov I G 1988 *Sov. J. Low. Temp. Phys.* **14** 149
[34] Farajian A A, Esfarjani K and Kawazoe Y 1999 *Phys. Rev. Lett.* **82** 5084
[35] Maksimenko A S and Slepyan G Y 2000 *Phys. Rev. Lett.* **84** 362
[36] Pop E, Mann D, Cao J, Wang Q, Goodson K and Dai H 2005 *Phys. Rev. Lett.* **95** 155505
[37] Perebeinos V, Tersoff J and Avouris Ph 2005 *Phys. Rev. Lett.* **94** 086802
[38] Mahan G D 2004 *Phys. Rev.* B **69** 125407
[39] Kane C L and Mele E J 1997 *Phys. Rev. Lett.* **78** 1932
[40] McEuen P L, Bockrath M, Cobden D H, Yoon Y-G and Louie S G 1999 *Phys. Rev. Lett.* **83** 5098
[41] Namiranian A, Kolesnichenko Yu A and Omelyanchouk A N 2000 *Phys. Rev.* B **61** 16796
[42] Bagheri M and Namiranian A 2006 unpublished
[43] Bruus H and Flensberg K 2004 *Many-Body Quantum Theory in Condensed Matter Physics* (New York: Oxford University Press)
[44] Anantram M P 2000 *Phys. Rev.* B **62** R4837
[45] Vukovic T, Miloevic I and Damnjanovic M 2002 *Phys. Rev.* B **65** 045418
[46] Esaki L 1957 *Phys. Rev.* **109** 603
[47] Tsu R and Esaki L 1973 *Appl. Phys. Lett.* **22** 562
[48] McEuen P L, Fuhrer M S and Park H 2002 *IEEE Trans. Nanotechnol.* **1** (1)
[49] Suzuura H and Ando T 2006 *J. Phys. Soc. Japan* **75** 024703
[50] McCann E, Kechedzhi K, Falko V I, Suzuura H, Ando T and Altshuler B L 2006 *Phys. Rev. Lett.* **97** 146805
[51] Davies J H 1998 *The Physics of Low-dimensional Semiconductors* (Cambridge: Cambridge University Press)
[52] Tersoff J and Hamann D R 1985 *Phys. Rev.* B **31** 805
[53] Wildöer J W G, Venema L C, Rinzler A G, Smalley R E and Dekker C 1998 *Nature* **391** 59
[54] Odom T W, Huang J L, Kim P and Lieber C M 1998 *Nature* **391** 62

J. Phys.: Condens. Matter **19** (2007) 469001 (1p) doi:10.1088/0953-8984/19/19/469001

Corrigendum

Effects of band structure and quantum interference on the differential conductance of infinite metallic single-wall carbon nanotubes

M Bagheri and A Namiranian 2007 *J. Phys.: Condens. Matter* **19** 469001

Published 02 November 2007
Online at stacks.iop.org/JPhysCM/19/469001

Recently we found that there was a missing factor, $\hbar v_F/2$, in the denominator of the amplitudes in equations (30) and (32). The correct equations are, respectively,

$$\Re\left[\frac{G_{\rm imp}^{\alpha\alpha,{\rm arm}}(V_{\rm sd},\mathcal{E}_{\mathcal{F}})}{G_0}\right]=\left(\frac{\pi g^2 T^{\rm arm}}{\hbar v_{\rm F}\mathcal{M}\mathcal{N}_{\rm arm}^2}\right)\cos\left[2k_{\rm F}(l_2-l_1)T^{\rm arm}\right]\times\cos\left[\left(\frac{eV_{\rm sd}}{\hbar v_{\rm F}}\right)(l_2-l_1)T^{\rm arm}\right],$$

and

$$\Re\left[\frac{G_{\rm imp}^{\alpha\alpha,{\rm zig}}(V_{\rm sd},\mathcal{E}_{\mathcal{F}})}{G_0}\right]=\left(\frac{\pi g^2 T^{\rm zig}}{\hbar v_{\rm F}\mathcal{M}\mathcal{N}_{\rm zig}^2}\right)\cos\left[\left(\frac{eV_{\rm sd}}{\hbar v_{\rm F}}\right)(l_2-l_1)T^{\rm zig}\right].$$

This factor just rescales the absolute value of the amplitudes by $2/\hbar v_{\rm F}\approx 0.1634$, and it does not affect anything else. Also, some misprinted errors have been detected:

(1) $g=10^3\gamma_0$, on page 11 after equation 33, should be replaced by $g=10^4\gamma_0$;
(2) All 'bohr' should be replaced by 'Bohr';
(3) $\tilde{g}^{\pm}$ in equation (23) should be replaced by $\mathbf{g}^{\pm}$.

These errors do not affect the conclusions of the paper. We apologize for these mistakes and any possible inconvenience they have caused.

